International Journal of Image and Graphics
Vol. 7, No. 1 (2007) 87-104
@World Scientific Publishing Company

# FAST ANALYTICAL RECONSTRUCTION OF GATED CARDIAC SPECT WITH NON-UNIFORM ATTENUATION COMPENSATION

YI FAN*
Department of Electronic Information
NorthWestern Polytechnical University
Xi'an, Shaanxi 710071, P. R. China
Email: fanyi618@126.com

HONGBING LU†
Department of Computer Applications/BME
Fourth Military Medical University
Xi'an, Shaanxi 710032, P. R. China
Email: luhb@fmmu.edu.cn

CHONGYANG HAO
Department of Electronic Information
NorthWestern Polytechnical University
Xi'an, Shaanxi 710071, P. R. China

ZHENGRONG LIANG
Department of Radiology, State University of New York
Stony Brook, NY 11794, USA

ZHIMING ZHOU
Department of Computer Applications/BME
Fourth Military Medical University
Xi'an, Shaanxi 710032, P. R. China

Conventionally, the inverse problem of gated cardiac SPECT is solved by reconstructing the images frame-by-frame, ignoring the inter-frame correlation along the time dimension. To compensate for the non-uniform attenuation for quantitative cardiac imaging, iterative image reconstruction has been a choice which could utilize an *a priori* constraint on the inter-frame correlation for a penalized maximum likelihood (ML) solution. However, iterative image reconstruction in the 4D space involves intensive computations. In this paper, an efficient method for 4D gated SPECT reconstruction is developed based on Karhune-Loève (KL) transform and Novikov's inverse

* First author.
† Corresponding author.

formula. The temporal KL transform is first applied on the data sequence to de-correlate the inter-frame correlation and then the 3D principal components in the KL domain are reconstructed frame-by-frame using Novikov's inverse formula with non-uniform attenuation compensation. Finally an inverse KL transform is performed to obtain quantitatively-reconstructed 4D images in the original space. With the proposed method, 4D reconstruction can be achieved at a reasonable computational cost. The results from computer simulations are very encouraging as compared to conventional frame-by-frame filtered back-projection and iterative ordered-subsets ML reconstructions. By discarding high-order KL components for further noise reduction, the computation time could be further reduced.

*Keywords*: Gated SPECT; analytical reconstruction; Karhune-Loève (KL) transform; Novikov's inverse formula;

## 1. Introduction

Gated cardiac single photon emission computed tomography (SPECT) imaging has been widely used to evaluate cardiac motion and other functions. The acquired four-dimensional (4D) sinogram data have both inter-frame correlation among the time sequence and intra-frame correlation within each 3D frame. Currently the time sequence is usually reconstructed frame-by-frame using a conventional filtered back-projection (FBP) method, which ignores the temporal correlation, smoothes the noise by a low-pass spatially-invariant linear filter and lacks quantitative capability. The quantitative aspect can be improved by a frame-by-frame ordered-subsets expectation-maximization (OSEM) reconstruction [1], but the inter-frame information is still not utilized. For fully 4D reconstruction, research efforts have been devoted to include a penalty for a penalized maximum likelihood (pML) solution, where the intra- and inter-frame correlations are considered in the penalty, see for example [2]. This classic approach is attractive because it searches for a statistical optimal solution but has several drawbacks, e.g., the reconstruction is time consuming because the solution is numerically tractable only by iterative algorithms and furthermore the solution strongly depends on several freely-adjustable parameters in the penalty. An alternative approach has been explored by the use of the Karhune-Loève (KL) transform to address the temporal correlation, see for example [3].

The KL transform, also called principal component analysis, has been investigated for many years to de-correlate multi-spectral, multi-band or colored images as an initial process for further compression, de-blurring, or de-noising [4, 5]. Since the KL transform has the property of de-correlating the time sequence in the KL domain and rearranging the principal components according to their variances, Kao, *et al.* [6] applied the KL transform for pre-reconstruction temporal sinogram smoothing for dynamic PET (positron emission tomography) imaging by discarding the higher order principal components which are dominated by noise (i.e., larger variances). Wernick, *et al.* [7] employed it to seek a penalized weighted least-squares (PWLS) estimate of the entire sequence in the KL domain for a fast reconstruction of dynamic PET. Narayanan, *et al.* [3, 8] extended the above KL-based framework [6, 7] to gated SPECT and showed that it was almost equally effective as the 4D iterative pML reconstruction but much faster in computation.

By reviewing the previous work of using KL transform to de-correlate a dynamic data sequence for 4D tomographic reconstruction, it should be noted that the previous methods could be roughly classified into two groups. One applies temporal smoothing for noise reduction in the KL domain [6], followed by frame-by-frame image reconstruction in the original space. Since the reconstruction is performed in the image domain, compensation for quantitative SPECT is readily available [9]. The other group employs temporal KL transform first, then performs a frame-by-frame reconstruction in the KL domain and obtains the final image sequence by inverse KL transform. This later approach has been explored for dynamic PET and SPECT without compensation in the frame-by-frame reconstruction [6, 7], and the reconstruction is mainly based on the Radon transform. For quantitative SPECT, the reconstruction shall be based on the attenuated Radon transform. Inverting the attenuated Radon transform has been an open question for many years until the recent work of Novikov [10] and Kunyansky [11].

In this paper, we present a quantitative reconstruction scheme for gated SPECT sequence in the KL domain. In this scheme, the data sequence is considered as a 4D volume and the KL transform is applied along the time dimension. In the KL domain, all the principal components of 3D volume are reconstructed one-by-one based on the Novikov's formula which inverts the attenuated Radon transform exactly [10, 11]. Finally, inverse KL transform is performed to obtain the reconstructed image sequence in the original space.

The presentation of this work is organized as follows. The temporal KL transform of gated SPECT data sequence is introduced in Section 2. The quantitative reconstruction based on the Novikov's inverse formula in the KL domain is described in Section 3. Computer simulation studies with comparison to frame-by-frame FBP and iterative OSEM are shown in Section 4. Discussion and conclusion on this quantitative approach are presented in Section 5.

## 2. KL Transform of Gated SPECT Data Sequence

The acquired dynamic projection data sequence $y$ from gated cardiac SPECT can be expressed mathematically as the attenuated Radon transform of the source distribution function $\lambda$, which reflects the mean number of gamma photons emitted by a radiotracer injected into the patient's body. The dynamic imaging procedure can be simply modeled as [7]:

$$E[y] = H\lambda \tag{1}$$

where $y = \left[y_1^T, y_2^T, \cdots y_K^T\right]^T$, $\lambda = \left[\lambda_1^T, \lambda_2^T, \cdots \lambda_K^T\right]^T$, and $T$ denotes the transpose operation. Notation $y_k$ ($k$=1, 2,…, $K$, where $K$ is the total number of time frames sampled within the cardiac cycle) represents a $L\times1$ vector ($L$ is the number of sinogram data points for each frame) obtained by lexicographically ordering the sinogram data, and $\lambda_k$ represents a $N\times1$ vector ($N$ is the number of pixels of the source image for each frame). $H = diag\left[H_1, H_1, \cdots, H_1\right]$, where $H_1$ is the system matrix that applies to each

single frame of data, representing the spatial-temporal system matrix of size $LK \times NK$ .

Assume the measured time-activity curve at pixel (*i,j*) of gated cardiac SPECT is represented by:

$$\lambda_{i,j}^{time} = [\lambda_{i,j}^{1}, \lambda_{i,j}^{2}, \cdots, \lambda_{i,j}^{K}]^{T} \tag{2}$$

Element (*k,l*) of the time covariance matrix $P^{time}$ can be estimated from all the gated frames by:

$$\left[P^{time}\right]_{k,l} = \frac{1}{N-1}\sum_{i,j}\left(\lambda_{i,j}^{k} - \overline{\lambda}^{k}\right)\left(\lambda_{i,j}^{l} - \overline{\lambda}^{l}\right) \tag{3}$$

where $N=I*J$ is the total number of pixels in one frame and $\overline{\lambda}^{k}$ represents the estimated mean value of frame *k* by:

$$\overline{\lambda}^{k} = \frac{1}{N}\sum_{i,j}\lambda_{i,j}^{k} \quad . \tag{4}$$

By singular value decomposition, the eigenvectors *M* of $P^{time}$ can be obtained from:

$$P^{time} M^{T} = M^{T} \cdot V \tag{5}$$

where $V = diag\{v_1, v_2, \cdots, v_k, \cdots, v_K\}$ and $v_k$ denotes the *k*-th eigenvalue of $P^{time}$ .

By multiplying the time-activity of pixels one-by-one with *M*, the temporal KL transform of the gated data can be performed by:

$$A = M \cdot \lambda_{i,j}^{time} \tag{6}$$

where $A_{i,j} = \left[a_{i,j}^{1}, a_{i,j}^{2}, \cdots, a_{i,j}^{K}\right]^{T}$ and $a_{i,j}^{k}$ is the *k*-th KL domain element at pixel (*i,j*). The KL transformed sequence then can be obtained by organizing $A_{i,j}$ for the corresponding pixels (*i,j*) in the KL domain. Since the KL transform is applied along the time dimension and the mean of each frame is computed from all *N* pixels in that frame using equation (4), all these *N* pixels are subjected to the same transformation.

To express the temporal KL transform of the entire dynamic sequence in a matrix format, we define $M_L$ by:

$$M_L = M \otimes I_L \tag{7}$$

where $I_L$ is the $L \times L$ identity matrix and $\otimes$ is the Kronecker product. By multiplying $M_L$ to both sides of the system model (1) and following the same schedule given by [7], we have:

$$\begin{aligned} M_L E[y] &= M_L H\lambda = (M \otimes I_L)(I_K \otimes H_1)\lambda \\ &= (MI_K) \otimes (I_L H_1)\lambda = (I_K M) \otimes (H_1 I_N)\lambda \\ &= (I_K \otimes H_1)(M \otimes I_N)\lambda = HM_N\lambda . \end{aligned} \tag{8}$$

If we define KL transformed data with:

$$\tilde{\lambda} = M_N \lambda, \quad and \quad \tilde{y} = M_L y. \tag{9}$$

The relationship between transformed gated projection data and transformed image sequence can be reflected by:

$$E[\tilde{y}] = H\tilde{\lambda} \tag{10}$$

Please note that (10) has the same form as (1), which indicates that the KL domain model is the same as that in the original (or spatio-temporal) domain. Since the system matrix H is exactly the same in both situations, the Novikov's inverse formula, which was derived for attenuation-compensated reconstruction in the spatial domain, could also be applied directly for reconstruction in the KL domain. It shall be noted that inverting both the Radon transform and the attenuated Radon transform is performed in the sinogram domain and does not trace any effect in the image domain. So is the presented inversion in the KL domain, where there is no any ray tracing between the image source and the acquired data.

## 3. Quantitative Reconstruction by Novikov's Inverse Formula in the KL Domain

Practical SPECT system suffers from many degradation factors, such as non-uniform attenuation, collimator blurring and scatter. Among them, inverting the attenuated Radon transform is the essential task for quantitative SPECT, though recent work from Gullberg's group [12], Tsui's group [13, 14], Qi's effort [15] and our group [16] suggests that compensation for degradation effects of scatter and collimator blurring is quite beneficial. In this study, since the major goal was to investigate the feasibility of inverting the attenuated Radon transform in the KL domain for 4D reconstruction, other degrading effects of scatter and collimator blurring are not considered. Novikov's explicit inverse formula offers us a way to solve the inverse problem in an analytical manner [10]. Detailed description of the Novikov's formula in a parallel-beam geometry and its implementation are given in [10, 11, 17]. Its extension to fan-beam, varying focal length fan-beam and other non-parallel beam geometries by various strategies can be found in [18-22]. In the following, we present our KL-domain Novikov's inverse formula in a parallel-beam geometry for simplicity.

Let $(x,y)$ be the stationary coordinate in the image domain and $(t,\theta)$ be the rotation coordinate in the sinogram space. As shown in the last paragraph of Section 2, the Novikov's formula could be used directly in the KL-domain. Following the analysis in [10, 11, 17], the KL domain Novikov's inverse formula can be expressed as:

$$\phi(\vec{r}) = \frac{1}{4\pi} div \int_0^{2\pi} \vec{j}\left[\exp\left([D\mu]_\theta(s,t)\right)\tilde{q}(t,\theta)\right]\Big|_{\substack{s=\vec{r}\bullet\vec{j}\\ t=\vec{r}\bullet\vec{k}}} d\theta \tag{11}$$

where $\vec{j} = (\cos\theta, \sin\theta)$, $\vec{k} = (-\sin\theta, \cos\theta)$, ***div*** is the divergence operation, $\phi(\vec{r})$ is the reconstructed image frame from its corresponding sinogram data frame $A(t,\theta)$ in the

KL domain and

$$\tilde{q}(t,\theta) = e^{-h_1}\{\cos(h_2)\tilde{q}_1(t,\theta) + \sin(h_2)\tilde{q}_2(t,\theta)\} \tag{12}$$

$$\tilde{q}_1(t,\theta) = \hat{H}\cos(h_2)e^{h_1}A(t,\theta) \tag{13}$$

$$\tilde{q}_2(t,\theta) = \hat{H}\sin(h_2)e^{h_1}A(t,\theta) \tag{14}$$

with $h_1 = \frac{1}{2}[R\mu](t,\theta)$, $h_2 = [\hat{H}h_1](t,\theta)$. The operators $\hat{H}$, $D$, and $R$ represent the Hilbert transform, the divergent beam transform, and the Radon transform, respectively, and are defined as follows:

$$[\hat{H}g](s) = \frac{1}{\pi}\int_{-\infty}^{+\infty}\frac{g(\tau)}{s-\tau}d\tau \tag{15}$$

$$[D\mu]_\theta(s,t) = \int_t^\infty \mu_\theta(s,\tau)d\tau \tag{16}$$

$$[R\mu](s,\theta) = \int_{-\infty}^{\infty}\mu_\theta(s,t)dt \tag{17}$$

The above quantitative reconstruction is performed frame-by-frame in the KL domain for each principal component, which is similar to that performed in the spatial domain, and the result is $\Phi_{m,n} = (\phi^1_{m,n}, \phi^2_{m,n}, \cdots \phi^l_{m,n}, \phi^{l+1}_{m,n}, \cdots, \phi^K_{m,n})$ for each image pixel ($m$,$n$) in the KL domain. Since the higher-order components with smaller eigenvalues may have little information, only the resulted frames reconstructed from the first $l$ low-order components, i.e. $\Phi^l_{m,n} = (\phi^1_{m,n}, \phi^2_{m,n}, \cdots \phi^l_{m,n})$ ($l \le K$), could be retained for further noise reduction and computing efficiency. After Novikov's inversion in the KL domain, an inverse KL transform on the $K$ or $l$ reconstructed frames will generate the gated images in the original space of

$$\hat{\lambda}^{time}_{m,n} = M^T\Phi \quad . \tag{18}$$

The presented analytical reconstruction of 4D gated cardiac SPECT sequence with non-uniform attenuation compensation is summarized below.

- Perform KL transform along the time projection sequence by equation (6) to de-correlate the inter-frame correlation and rearrange the data signal-to-noise ratios (SNRs) according to the eigenvalues of the KL principal components. The higher-order components with smaller eigenvalues may be discarded for further reduction of both noise and computing time.
- Reconstruct each of the remaining KL components by equation (11), where the non-uniform attenuation is accurately compensated and the computation can be parallelized for simultaneous reconstruction of all the KL components.
- Perform inverse KL transform on the reconstructed KL components by equation (18) to obtain the gated SPECT image sequence.

## 4. Experimental Results

Computer simulations were conducted to show the feasibility of the presented analytical reconstruction for quantitative gated SPECT and its potential in practical use. The simulation studies were based on the 4D mathematical torso phantoms with cardiac gating along the time dimension and defects inside the myocardium (gMCAT and gNCAT) [23]. The relative activity levels of the heart: lungs: liver: kidney: spleen: sternum were 1.0: 0.03: 0.69: 0.84: 0.96: 0.12, respectively, simulating the distribution of $Tc^{99m}$ concentration in these organs [23]. The torso attenuation map was specified by the given organs and their locations inside the body. A dynamic sequence consisting of 16-interval gated activity distributions each of 128 cubic size was generated in which the radiotracer distribution changes with time, simulating the ground truth. Noise-free projection data or sinogram from each of the 16 ground-true frames was computed by tracing the activity distribution of the given organs through the given attenuation map. Each sinogram had a volume size of 128 cubic with 128 angular samples evenly spaced on 360 degrees. Since scatter and collimator blurring were not considered in this study, the intra-frame 3D data processing was essentially a 2D operation. For simplicity, a 2D process on a 128x128 slice of the torso phantom was described below.

Focusing on a 2D slice of the torso gNCAT phantom, Table 1 shows the eigenvalue distribution for the first four components individually and their accumulated summations over the sum of all eigenvalues. The first component took 96.05% of the total eignvalues. The second one took only 3.5% of the total eigenvalues. The summation of the first 4 components took 99.94% of the total eigenvalues. It is clearly seen that the first four principal components contain almost the entire information of the 16 gated frames. The remaining 12 higher-order components would be very noisy with little information and could be discarded for further reduction of noise and computing time.

Table 1: Eigenvalues corresponding to the first four KL components.

| KL Component | % Total Eigen-values | % Sum of Total Eigen-values |
|---|---|---|
| 1 | 96.05 | 96.05 |
| 2 | 3.50 | 99.54 |
| 3 | 0.29 | 99.84 |
| 4 | 0.10 | 99.94 |

Five different reconstruction methods were compared: 1) frame-by-frame FBP reconstruction (“FBP”), 2) frame-by-frame OSEM reconstruction (“OSEM”), 3) frame-by-frame Novikov reconstruction (“Novikov”), 4) the proposed reconstruction from all the KL components (“KL-Novikov”), and 5) the proposed reconstruction from the first four principal components (“KL-Novikov-4”). Figure 1 shows the phantom used and the reconstructed images of frames 1, 6, 11, 14 and 16 with different reconstruction methods. To see the detailed distribution on the myocardium, a region of interest (ROI) was selected in this picture presentation. Table 2 reports the computational costs of different reconstruction methods.

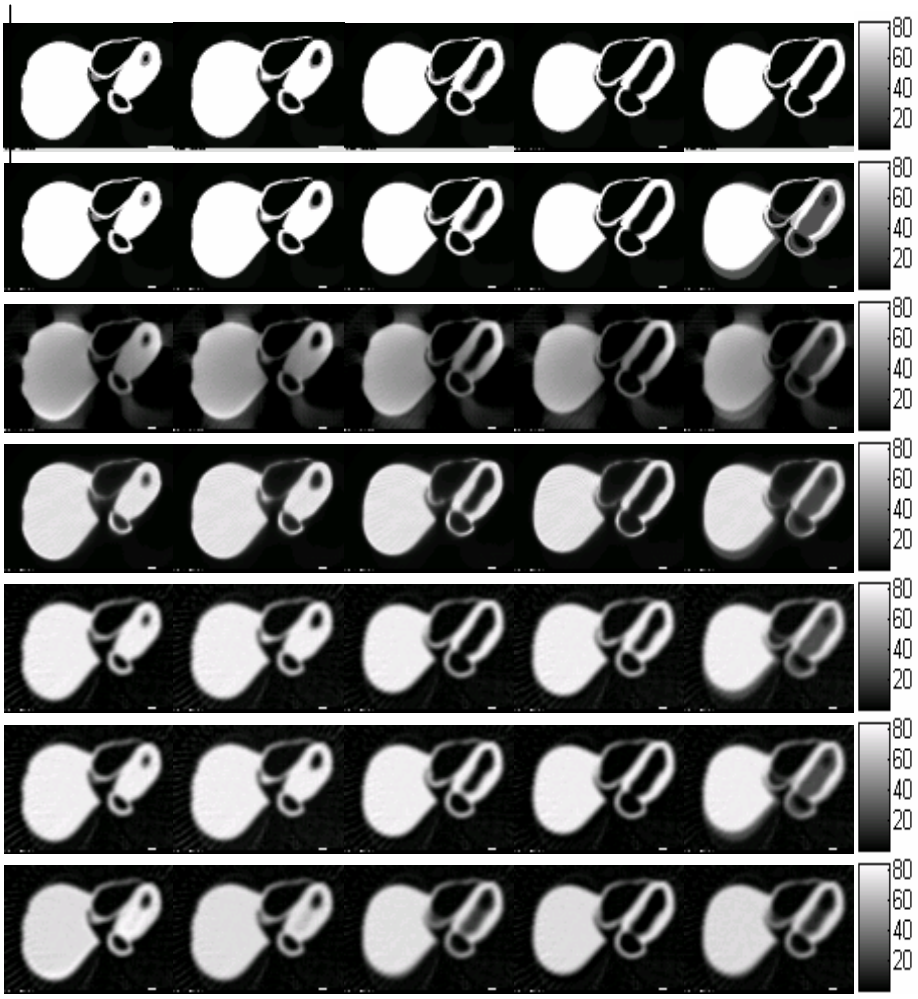


Figure 1: Temporal behavior of gated cardiac SPECT images reconstructed by different approaches for the gNCAT phantom in noise-free case. From left to right – a transverse slice from temporal frame 1, 6, 11, 14 and16. From top to bottom – activity phantom slice, temporal correlated phantom slice, reconstructed image slices by FBP, iterative OSEM (with 5 iterations for each frame and subset size of 8), Novikov's formula, and KL-Novikov reconstruction from all the KL components and from the first four components.

Table 2: Computational cost of different reconstruction approaches.

| Method | Computation Cost | Computation Time(s) |
|---|---|---|
| FBP | 16 FBP | 15 |
| OSEM | 90 iterations | 66 |
| Novikov's inversion | 16 inversions | 29 |
| KL-Novikov of all components | KL transform + 16 inversions | 31 |
| KL-Novikov of the first four components | KL transform + 4 inversions | 12 |

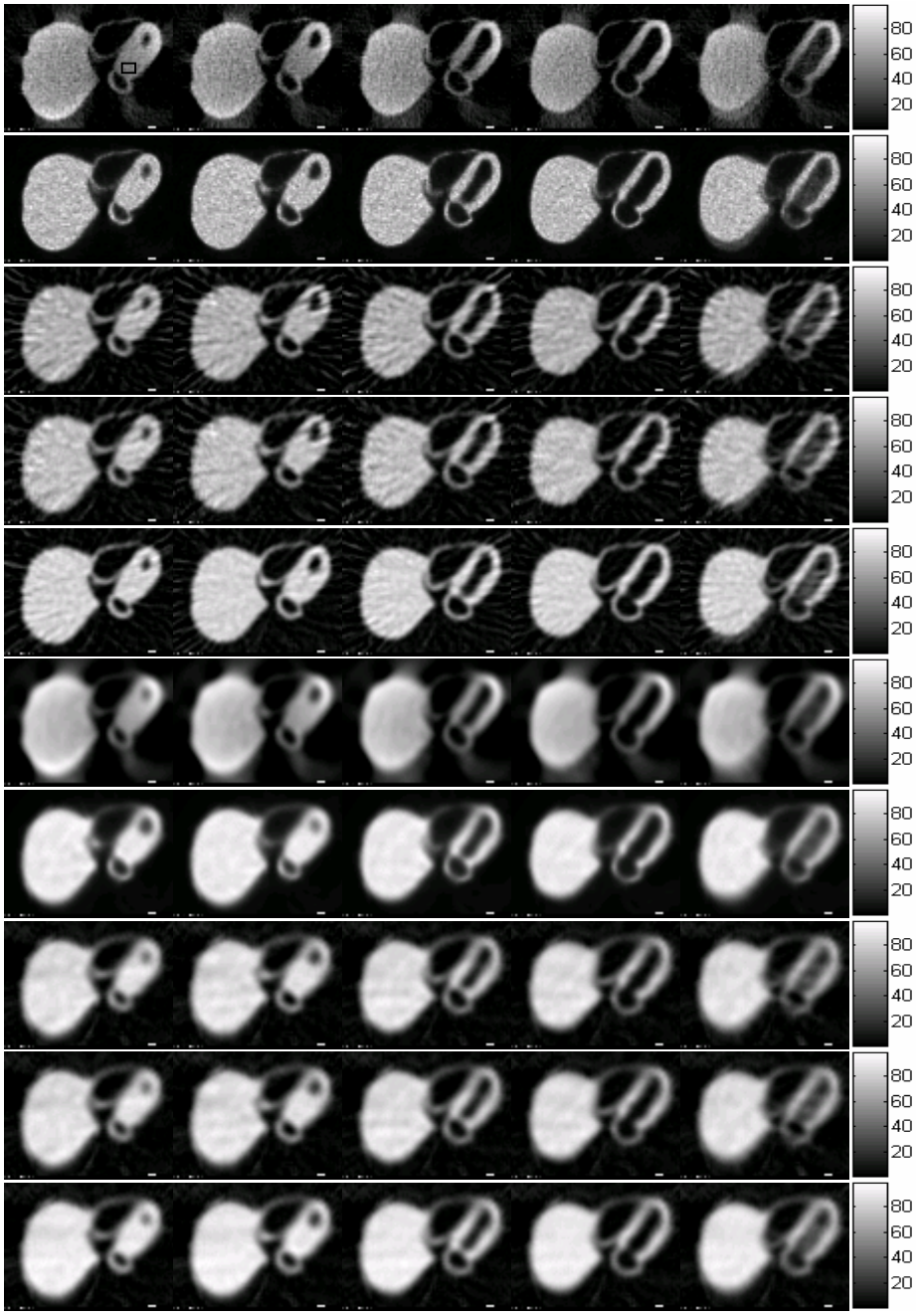


Figure 2: Temporal behavior of gated cardiac SPECT images reconstructed by different approaches for the gNCAT phantom in noisy case. From left to right – a transverse slice from temporal frame 1, 6, 11, 14 and 16. From top to bottom of the first 5 row – reconstructed image with non-filtering strategy slices by FBP,

OSEM(with 5 iterations for each frame and subset size of 8), Novikov's formula, and KL-Novikov reconstruction from all the KL components and from the first four components. From top to bottom of the last 5 row – reconstructed image with pre-filtered by Hanning filter of cutoff frequency 0.5 strategy slices by FBP, OSEM (with 5 iterations for each frame and subset size of 8), Novikov's formula, and KL-Novikov reconstruction from all the KL components and from the first four components.

The standard FBP reconstruction frame-by-frame with ramp filter at the Nyquist frequency cutoff took a total of 15 seconds on a PC with 1.5GHz CPU and 1.0GB RAM. Since it did not compensate for the attenuation, the reconstructed images show expected density variation on a uniformly distributed region. The iterative OSEM converged quickly to a stable estimate after 5 iterations. The total of 90 iterations for the 16 gated frames cost a total of 66 seconds. Due to its capability to compensate for the attenuation, OSEM generated quite good results. However, some density variation on a uniformly distributed region was seen because of its non-uniform convergence behavior across the field-of-view (FOV). This observation on OSEM reconstruction is consistent with the previous studies, see for example [24]. Applying the Novikov's inverse formula of equation (6) directly to each of the 16 sinogram frames also generated very good results. The total time cost was 29 seconds, with a significant reduction on computing time over the OSEM. The presented KL-Novikov inversion on all the 16 frames took 31 seconds. By discarding the higher-order components (only the first four components reserved), the presented quantitative inversion for gated SPECT reconstruction of 16 frames only took 12 seconds.

It is noted that the first row of Figure 1 was generated directly from gNCAT phantom. Since there is no correlation present between slices of neighboring frames, "temporal correlated phantom slices", shown in the images of the second row of Figure 1, were generated by weighted averaging (0.1:0.2:0.4:0.2:0.1) of 5 consecutive phantom slices. In this noise-free case, the KL transform offered limited benefit to gated studies visually. However, all the quantitative inversion results showed excellent uniformity for a uniform source region across the FOV. To simulate noisy cases, Poisson noise was added to ideal sinograms generated. The total count was 20K per view, and the reconstructed slices are shown in Figure 2. The inversion without KL transform had a higher noise level compared to the inversion with KL transform. More noise reduction was observed by discarding the higher-order components

To assess and compare the regional performance of the above five reconstruction schemes, the regional bias-variance plots are generated. The bias and variance estimates were calculated for each of the five schemes as follows:

$$Bias(\%) = 100(B_z(ROI)/Z(ROI)) \tag{19}$$

$$Variance\ (\%) = 100\,(V_z(ROI)/Z^2(ROI)) \tag{20}$$

where

$$B_Z(ROI) = \frac{1}{L}\sum_{j=1}^{L}(Z^j(ROI) - Z(ROI)) \tag{21}$$

$$V_Z(R) = \frac{1}{L-1}\sum_{j=1}^{L}(Z^j(ROI) - \overline{Z}(ROI))^2 \tag{22}$$

and $Z^j(ROI) = \frac{1}{L_R}\sum_{i\in ROI} f_i^j$, $L$ is the number of realization, $L_R$ is the number of pixels in that region. Notation $f_i^j$ represents the reconstructed distribution value of pixel $i$ in the $j$ th realization. $\bar{Z}(ROI) = \frac{1}{L_R}\sum_{i\in ROI} f_i$ is the mean value of the true image in the ROI, and $\overline{Z}(ROI)$ is the mean of $Z^j(ROI)$.

In this study, 200 realization of the gNCAT phantom with Poisson noise were simulated. A regions include 24 pixels located within the left ventricular wall (marked on the left-top image of Figure 2) was selected to calculate regional bias and variance. In order to establish more comprehensive evaluation, both non-filtering strategies and pre-filtering strategies (which filters the projection data by the Hannning with cutoff frequency 0.5 before reconstruction) for all the five reconstruction methods were carried out.

The region bias-variance plots are show in Figure 3 and Figure 4 for the non-filtering and pre-filtering strategies, respectively. The KL-Novikov with all components obtained almost the same results with that of Novikov, so it was not shown in the figures. Note that KL-Novikov with the first four components (KL-Novikov-4) obtained the best results for all the strategies.

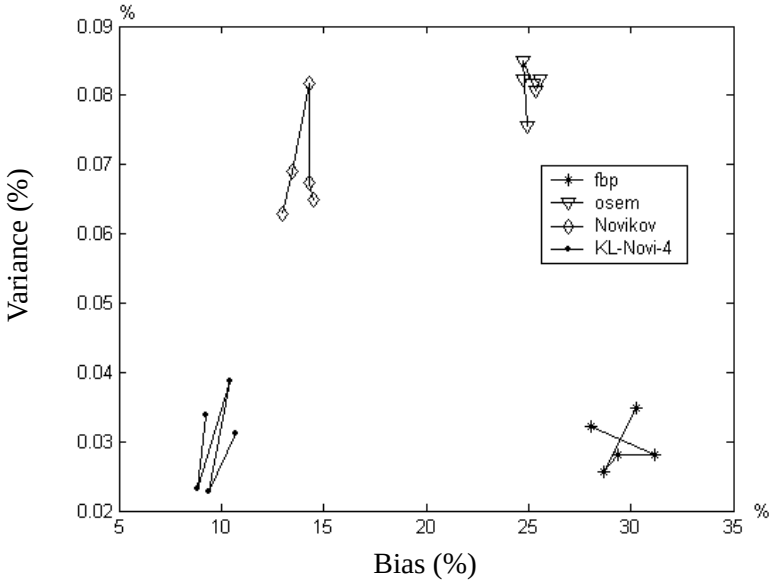


Figure 3: Bias-variance plot of given ROI in reconstructed image of frame 1, 6, 11, 14, and 16 for non-filtering strategy.

The second simulation study was based on the gMCAT torso phantom with defects inside the myocardium. The relative activity levels of different organs are

similar to those of gNCAT phantom. The gated sequences were generated with no spatial variance. Similar simulation and reconstruction procedures to the study using the gNCAT phantom were repeated here for the gMCAT phantom. The results for noise-free case are shown in Figure 5, while the results for noisy cases are shown in Figure 6. To more quantitatively demonstrate the detectability of defects using different reconstruction methods, horizontal density profiles through the defect for the first frame were also given as the first column.

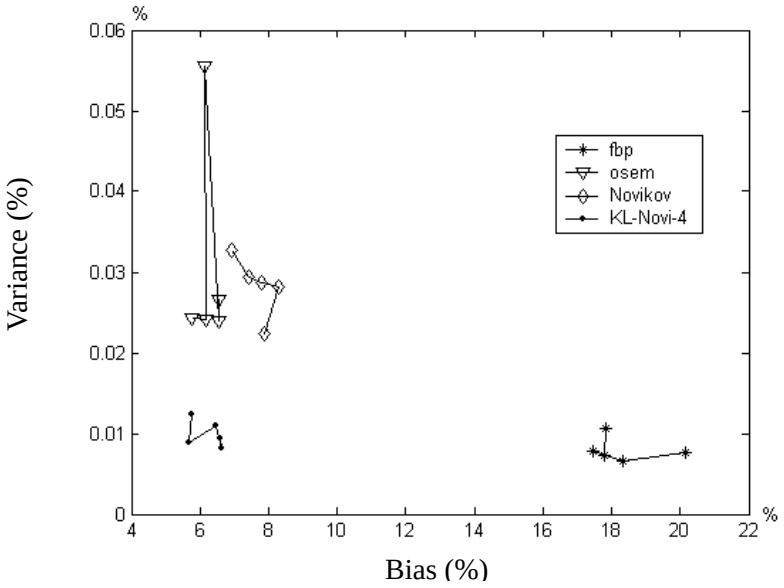


Figure 4: Bias-variance plot of given ROI in reconstructed image of frame 1, 6, 11, 14, and 16 for pre-filtering strategy.

To save more computing time, we even discarded more higher-order principal components. Only the first two components were used for fast reconstruction. A similar conclusion to the use of four components can be drawn from the results of Figure 5 in noise-free cases and that of Figure 6 in noisy cases. From the intensity profiles in Figures 5 and 6, we can see that for lesion detectability, the OSEM, KL-Novikov and Novikov have a similar performance, outperforming the conventional FBP method.

From above simulation results, it can be noticed that the inversion results show some streak artifacts around borders compared to iterative approaches. To demonstrate the influence of streak artifacts on lesion detectability, Figure 7 gives a density profile along a vertical line between the left border and the liver (marked on the left-top image of Figure 1). It shows that due to unoptimizable implementation of the inverse formula given in equation (11), the density value reconstructed from Novikov's method fluctuates greater along the true value compared to iterative methods, which may reduce the detectability in border regions.

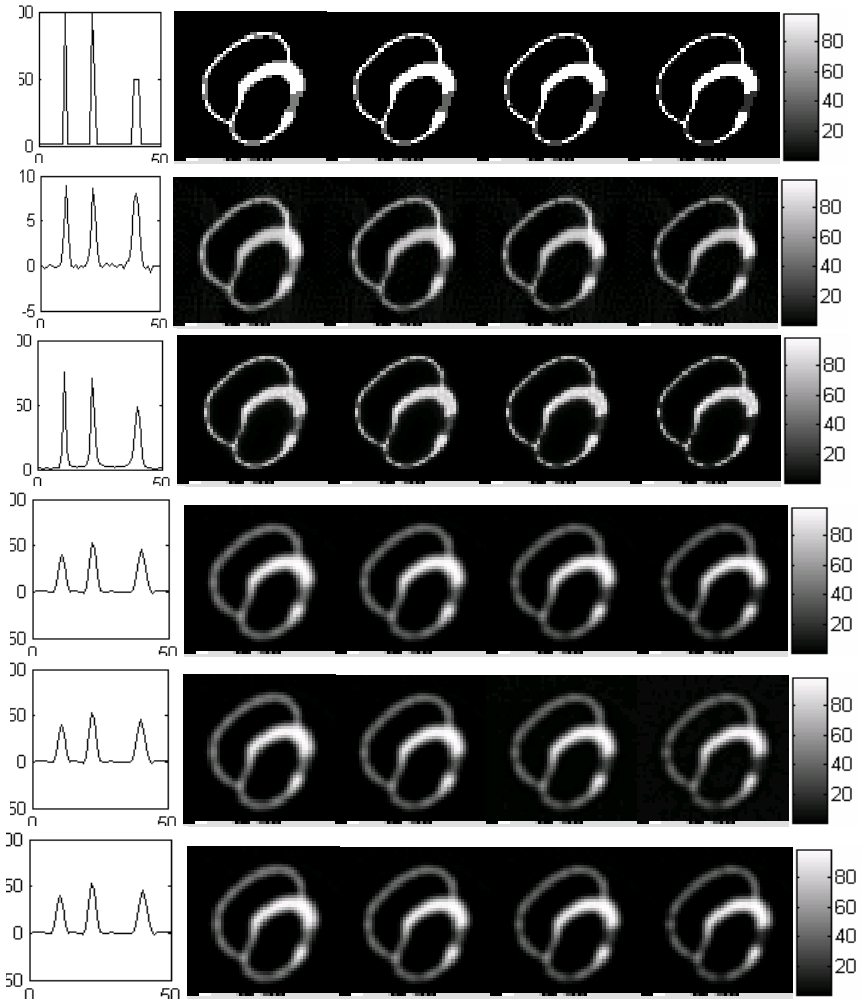

Figure 5: Temporal behavior of gated cardiac SPECT images reconstructed by different approaches for the gMCAT phantom in noise-free case. From left to right: density profile of frame 1 through the defect (the horizontal line is marked on the first profle), transverse slices from temporal frame 1, 5, 11and 16. From top to bottom: activity phantom, reconstructed image slices by FBP (no attenuation compensation), OSEM (with 5 iterations for each frame and subset size of 8), Novikov's formula, and KL-Novikov reconstruction from all the KL principal components and from the first 2 components.

## 5. Discussion and Conclusion

In this paper, an analytical reconstruction scheme for quantitative gated SPECT was presented. The temporal correlation among the gated sequence of sinogram frames was considered by the KL transform. In the KL domain, the higher-order principal components with smaller eigenvalues could be discarded for reduction of

both noise and computing time. Quantitative inversion with the principal component analysis demonstrated improvement in noisy case over the quantitative inversion without the KL transform.

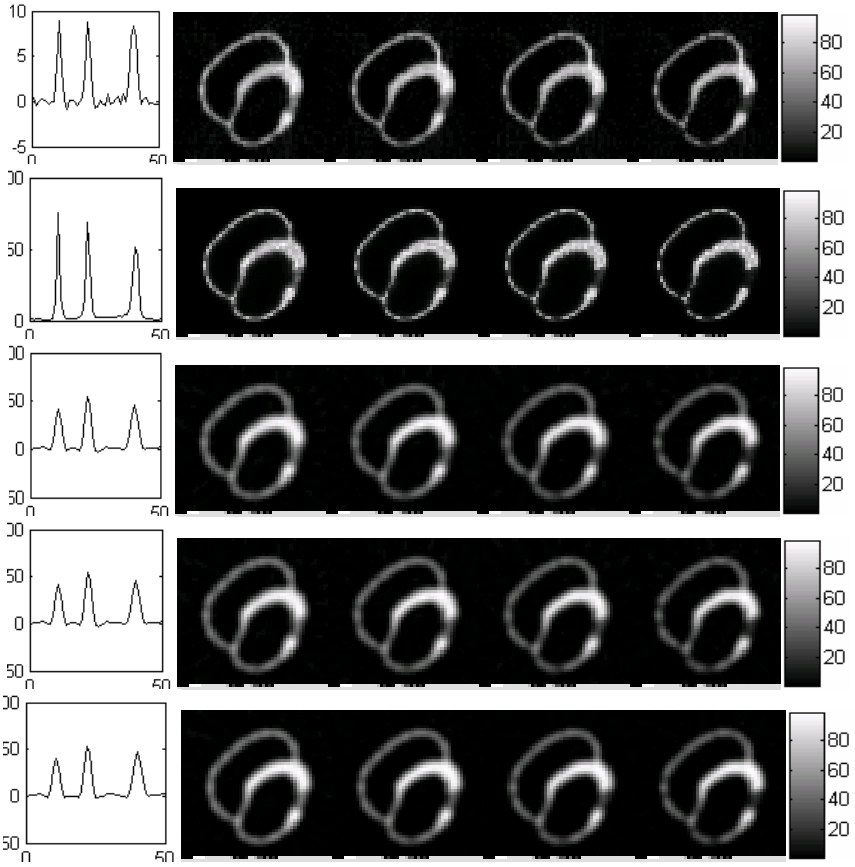


Figure 6: Temporal behavior of gated cardiac SPECT images reconstructed by different approaches for the gMCAT phantom in noisy case. From left to right: density profile of frame 1 through the defect (the horizontal line is marked on the first profle), transverse slices from temporal frame 1, 5, 11and 16. From top to bottom – reconstructed image with non-filtering strategy slices by FBP, OSEM (with 5 iterations for each frame and subset size of 8), Novikov's formula, and KL-Novikov reconstruction from all the KL components and from the first two components.

The presented analytical reconstruction of gated SPECT has several advantages over the conventional FBP method such as (1) having quantitative capability by compensating for the non-uniform attenuation and (2) being more effective in noise reduction because of the unique SNR distribution among the KL principal components, where the noise treatment can be adaptive to each component [9, 25]. Compared to the well-known OSEM, the presented inversion approach is computationally efficient and

has a more consistent performance on resolution uniformity across the FOV.

The presented analytical inversion approach also has several drawbacks compared to iterative pML reconstruction. Due to the band-limited sampling of the data and an imposed frequency cutoff either explicitly or implicitly in the inversion process (depending on different implementations of the inverse formula of equation (11) [11, 21]), the inversion results show some streak artifacts around borders, as shown in Figure 7, and somewhat smoothed edge compared to that of iterative approaches. More effort should be devoted to improve the practical performance of the Novikov's inverse formula. In general, a mathematically-rigorous inversion is less tolerant than an iterative approach on data sampling error, noise and incompleteness. Therefore, more powerful filtering strategy should be utilized when the Novikov's inverse formula is involved in an analytical approach to quantitative SPECT image reconstruction.

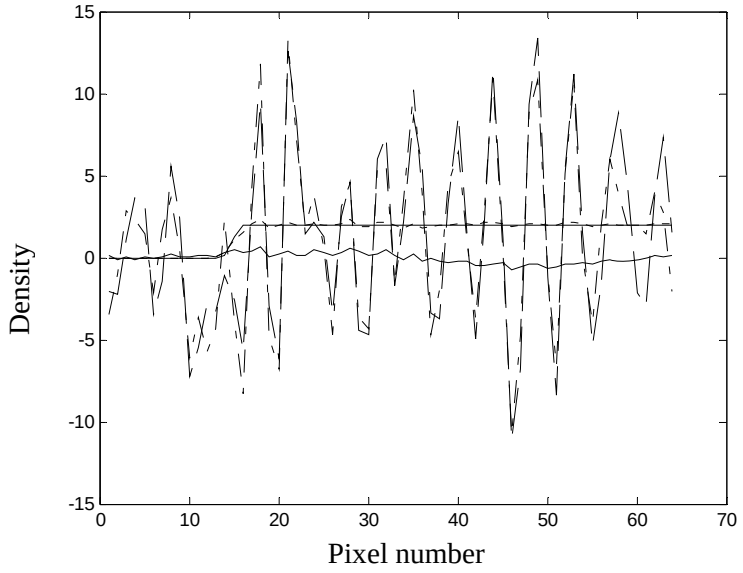


Figure 7: Density profile along a vertical line between the left border and the liver (marked on the left-top image of Figure 1). Upper solid line -- phantom density; lower solid line – FBP; dotted line – OSEM; dashed line – Novikov; and dash-dot line – KL-Novikov-4.

In the presented KL-transform along the time sequence, time covariance matrix was computed using all pixels in each frame. In other words, all the pixels in each frame underwent the same transformation. This may add in more edge blurring in the inversion results. This drawback could be mitigated by clustering the pixels into subgroups and applying spatially-variant KL transform on each subgroup, as proposed in [26]. This adaptive KL transform strategy and other possible solutions are currently under investigation.

As we noted before, the practical SPECT systems also suffer from other degradation factors, such as depth dependent blurring and scatter. For quantitative

reconstruction, appropriate compensation for those factors should also be included into the analytical framework. In this present study, our major goal is to investigate the feasibility of FBP-type solution in the KL domain for 4D reconstruction. Therefore, only the inversion of the attenuated Radon transform was considered in the imaging model. The preliminary results shown in this paper can be regarded only as quasi-quantitative. An analytical framework based on more realistic imaging model, including the depth dependent blurring and scatter, should be developed for quantitative gated SPECT in the future.

## Acknowledgements

We would like to thank the anonymous reviewers for their very careful reading of the text and valuable comments. This work was supported in part by the National Natural Science Foundation of China under Grant No. 30170278 and 30470490. Dr. Liang was supported by the NIH National Cancer Institute under Grant # CA82402.

## References

1. H.M. Hudson and R.S. Larkin, "Accelerated image reconstruction using ordered subsets of projection data", *IEEE Trans. Med. Imaging*, vol. 13, pp. 601-609, 1994.
2. D.S. Lalush and B.M.W. Tsui, "Block iterative techniques for fast 4D reconstruction using *a priori* motion models in gated SPECT", *Phys. Med. Biology*, vol. 43, pp. 875-886, 1998.
3. M.V. Narayanan, M.A. King, E.J. Soares, C.L. Byrne, P.H. Pretorius, and M.N. Wernick, "Application of the Karhunen-Loeve transform to 4D reconstruction of cardiac gated SPECT images", *IEEE Trans. Nucl. Science*, vol. 46, pp. 1001-1008, 1999.
4. D.C. Barber, "The use of principal components in the quantitative analysis of gamma camera dynamic studies," *Phys. Med. Biology*, vol. 25, pp. 283-292, 1980.
5. B.R. Hunt and O. Kübler, "K-L multi-spectral image restoration, part I: theory", *IEEE Trans. ASSP*, vol. 32, pp. 592-600, 1984.
6. C-M. Kao, J.T. Yap, J. Mukherjee, and M.N. Wernick, "Image reconstruction for dynamic PET based on low-order approximation and restoration of the sinogram", *IEEE Trans. Med. Imaging*, vol. 16, pp. 738-749, 1997.
7. M.N. Wernick, E.J. Insusino, and M. Milosevic, "Fast spatio-temporal image reconstruction for dynamic PET", *IEEE Trans. Med. Imaging*, vol. 18, pp. 185-195, 1999.
8. M.V. Narayanan, M.A. King, M.N. Wernick, C.L. Byrne, E.J. Soares, and P.H. Pretorius, "Improved image quality and computation reduction in 4-D reconstruction of cardiac-gated SPECT images", *IEEE Trans. Med. Imaging*, vol. 19, pp. 423-433, 2000.
9. H. Lu, G. Han, D. Chen, L. Li, and Z. Liang, "A theoretically based pre-reconstructing filter for spatio-temporal noise reduction in gated cardiac SPECT imaging", *Conference Record IEEE NSS-MIC*, in CD-ROM, 2000.
10. R.G. Novikov, "An inversion formula for the attenuated X-ray transformation", *Comptes Rendus de I'Académie des Science* (Series I-Mathematics), vol. 332(12), pp. 1059-1063, 2001, and in *Ark. Math.*, vol. 40, pp. 145-167, 2002.
11. L.A. Kunyansky, "A new SPECT reconstruction algorithm based on the Novikov's explicit inversion formula", *Inverse Problems*, vol. 17, pp. 293-306, 2001.
12. D.J. Kadrmas, E.V.R. DiBella, R.H. Huesman, and G.T. Gullberg, "Analytical propagation of errors in dynamic SPECT: estimators, degrading factors, bias and noise", *Phys. Med. Biology*, vol. 44, pp. 1997-2014, 1999.

13. S. Sankaran, E.C. Frey, K.L. Gilland, and B.M.W. Tsui, "Optimum compensation method and filter cutoff frequency in myocardial SPECT: a human observer study", *J. Nucl. Medicine*, vol. 43, pp. 432-438, 2002.
14. X. He, E.C. Frey, J.M. Links, K.L. Gilland, W.P. Segars, and B.M.W. Tsui, "A mathematical observer study for the evaluation and optimization of compensation methods for myocardial SPECT using a phantom population that realistically models patient variability", *IEEE Trans. Nucl. Science*, vol. 51, pp. 218-224, 2004.
15. J. Qi, ""Comparison of statistical reconstructions with isotropic and anisotropic resolution", *IEEE Nuclear Science Symposium and Medical Imaging Conference Record*, pp. 3624-3628, 2004.
16. T. Li, J. Wen, G. Han, H. Lu, and Z. Liang, "Evaluation of an efficient compensation method for quantitative fan-beam brain SPECT reconstruction", *IEEE Trans. Med. Imaging*, vol. 24, pp. 170-179, 2005.
17. F. Natterer, "Inversion of the attenuated Radon transform", *Inverse Problems*, vol. 17, pp. 113-119, 2001.
18. J. Wen, T. Li, and Z. Liang, "Ray-driven analytical fan-beam SPECT reconstruction with non-uniform attenuation", *IEEE International Symposium on Biomedical Imaging*, pp. 629-632, 2002.
19. J. Wen, T. Li, and Z. Liang, "An analytical inversion of non-uniformly attenuated Radon transform for SPECT reconstruction with variable focal-length fan-beam collimators", *IEEE Trans. Nucl. Science*, vol. 50, pp. 1541-1549, 2003.
20. J. You, G.L. Zeng, and Z. Liang, "FBP algorithms for attenuated fan-beam projections", *Inverse Problems*, vol. 21, pp. 1179-1192, 2005.
21. T. Li, J. You, J. Wen, and Z. Liang, "An efficient reconstruction method for non-uniform attenuation compensation in non-parallel beam geometries based on Novikov's explicit inversion formula", *IEEE Trans. Med. Imaging*, vol. 24, pp. 1357-1368, 2005.
22. Q. Huang, G.L. Zeng, J. You, and G.T. Gullberg, "A cone-beam reconstruction algorithm for non-uniformly attenuated projections acquired using a circular trajectory", *Phys. Med. Biol.*, vol. 50, pp. 2329-2339, 2005.
23. P.H. Pretorius, W. Xia, M.A. King, *et al*., "Evaluation of right and left ventricular volume and ejection fraction using a mathematical cardiac torso phantom for gated pool SPECT", *Journal of Nuclear Medicine*, vol. 38, pp. 1528-1534, 1997.
24. C.L. Byrne, "Block-iterative methods for image reconstruction from projections", *IEEE Trans. Image Processing*, vol. 5, pp. 792-794, 1994.
25. H. Lu, D. Chen, G. Han, L. Li, and Z. Liang, "A combined transformation of ordering SPECT sinograms for signal extraction from measurements of Poisson noise", *SPIE Medical Imaging*, vol. 4322, pp. 943-951, 2001.
26. J.G. Brankov, Y. Yang, M. V. Narayanan, and M. N. Wernick, "Spatially adaptive temporal smoothing for reconstruction of dynamic PET and gated SPECT images," *IEEE Proc. of NSS and MIC*, vol. 2, pp. 146-150, 2000.

## Photo and Bibliography

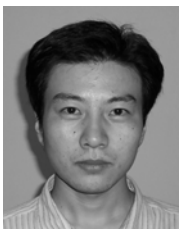

**Yi Fan** received the bachelor's degree from Xi'An Institute of Technology, China, in 1998 and Master's degree from Xi'An University of Technology, China, in electronic engineering, respectively. From 2003 till now, he is PhD candidate of NorthWestern Polytechnical University, Xi'An, China as well as academic research field in area of Digital Image Processing.

**Chongyang Hao** is currently a Professor and Director of Science of Signal and Informatics of NorthWestern Polytechnical University, Shaanxi, China. After graduated from the university in 1964, he has worked in the department of electronic engineering. From 1993 till 1995, he worked as visiting professor in Ruhr University, German. His research interests focus on virtual reality, image processing and graphics. He has authored more than 200 scientific publications and is the principal investigator of several projects. He is also the member of several committees on assessment of degree-award, National Science Foundation and Science Foundation of several provinces.

**Zhiming Zhou** is currently an Associate Professor and Senior Laboratory Assistant of the Computer Application Department in the Biomedical Engineering School, Fourth Military Medical University, Shaanxi, China. His research interests focus on signal processing. He has authored more than 50 scientific publications and edited 7 scientific literatures. From 2001 till 2006, he has participated in several project funded by the National Science Foundation and the Department of Defense of China.